Radiation Physics and Chemistry 175 (2020) 108077

Contents lists available at ScienceDirect

Radiation Physics and Chemistry

journal homepage: www.elsevier.com/locate/radphyschem

X-ray Absorption Spectroscopy investigations of disordered matter

Andrea Di Cicco

Physics Division, School of Science and Technology, University of Camerino, 62032 Camerino, MC, Italy

ARTICLE INFO

Keywords:
Liquid
Glasses
EXAFS
Disorder

ABSTRACT

X-ray Absorption Spectroscopy (XAS) is known to be an ideal technique for investigating matter lacking crystalline ordering. This work reports about present methods used for investigating disordered matter, discussing data-analysis and simulations strategies as well as several experimental techniques with applications. The current approach based on the comparison among multiple-scattering simulations associated with the *n*-body distribution functions and EXAFS (Extended X-ray Absorption Fine Structure) experimental data, including application of Reverse Monte Carlo methods, is discussed. Several studies of amorphous and liquid systems are presented, showing the potential of XAS in answering some important questions related to preferred local symmetries in liquid systems and presence of polymorphism in glasses and liquids. Experiments are presented discussing also the advances related to the performance of high-pressure and high-temperature experiments in disordered systems, highlighting the importance of combining XAS, x-ray diffraction and suitable diagnostics. XAS ability in measuring phase transitions and structure in undercooled metastable liquids is discussed. New possibilities offered by EXAFS measurements of light elements using inelastic scattering (x-ray Raman) are presented discussing the notable example of liquid water. Mention to new time-resolved applications at synchrotrons and free-electron lasers is also given.

1. Introduction

The x-ray absorption spectroscopy (XAS) technique is now recognized as an extremely powerful method for investigating the local atomic structure spanning the phase diagram of a variety of substances, including appearance of metastable and transient states. In particular, the oscillations of the x-ray cross-sections, commonly referred as EXAFS (Extended X-ray Absorption Fine Structure), can be used to obtain a reliable reconstruction of the short-range structure around selected atomic species. Due to those unique features, the importance of performing EXAFS experiments in disordered matter like glasses and liquids was soon understood (see Crozier et al., 1988 and refs. therein).

The development of advanced and reliable data-analysis approaches is one of the important aspects of the adoption of XAS as a technique of choice for structural determinations. The evolution from a simple plane-wave single-scattering approach to more accurate and reliable curved-wave multiple-scattering calculations started already since the late seventies. Advanced EXAFS data-analysis methods, based on multiple-scattering simulations evolving on continuously improved computing resources, were gradually developed in U.K. at Daresbury (EXCURVE Gurman et al., 1986 with later fitting implementations, EXCURV98), in Italy at Frascati (GNXAS Filipponi et al., 1991), and in U.S.A. at Seattle (FEFF Rehr et al., 1991, using fitting routines like FEFFIT Newville et al., 1995).

In particular, structural refinements of disordered systems required specific developments of data-analysis techniques, among which GNXAS Filipponi et al., (1991, 1995), Filipponi and Di Cicco (1995a), Di Cicco (2009) played a major role. The correct account of configurational disorder is one of the key points in treating non-crystalline systems and the extensive use of computer simulations (namely Monte-Carlo, Molecular Dynamics, and Reverse Monte-Carlo) was shown to improve our insight on the local structure in disordered substances.

Other crucial developments regarded the optimization of the synchrotron radiation sources, beamlines, sample environment with suitable diagnostics, allowing the performance of accurate XAS experiments under non-standard conditions of temperature and pressure, including also time-resolved studies (see for example Itié et al., 1997; Filipponi et al., 1998; Mathon et al., 2016 and refs. therein).

In this work, I shall briefly discuss advances in XAS techniques relevant for structural studies of disordered systems. Theoretical and computational methods are presented in Section 2, while examples and results of XAS experiments on disordered substances are briefly reported in Section 3.

E-mail address: andrea.dicicco@unicam.it.

https://doi.org/10.1016/j.radphyschem.2018.11.031
Received 23 October 2018; Received in revised form 12 November 2018; Accepted 29 November 2018
Available online 21 December 2018
0969-806X/

2. Modelling XAS of disordered matter

Modern approaches for EXAFS structural refinement are based on the comparison of experimental data with multiple-scattering simulations. As previously mentioned, GNXAS (Filipponi et al., 1991) was specifically developed to deal with disordered systems. In fact, the theory incorporated within the GNXAS (*n*-body expansion) method (Filipponi et al., 1995, 1991; Filipponi and Di Cicco, 1995a; Di Cicco, 2009) is ideally suited for a correct application of the configurational average in a generic disordered system through the *n*-body distribution functions (pair, triplet and so on). The fundamental equation relating the *n*-body (n = 2,3,…) distribution functions $g_n(\{r\})$ ({r} being a set of coordinates defining *n*-atom configurations) and XAS is the following:

$$\chi_\alpha(k) = \sum_\beta \int_0^\infty 4\pi\rho_\beta r^2 g_2^{\alpha\beta}(r)\gamma_\beta^{(2)}(k,r)dr + \sum_{\beta\beta'} \int d\eta_1 dr_2 d\theta\ 8\pi^2 r_1^2 r_2^2 \sin(\theta)\rho_\beta\rho_{\beta'}\times g_3^{\alpha\beta\beta'}(r_1, r_2, \theta)\,\gamma_{\beta\beta'}^{(3)}(r_1, r_2, \theta, k) + \cdots \quad (1)$$

The XAS signal $\chi_\alpha(k)$, related to a selected core excitation of the α chemical species, is a function of the photoelectron wave-vector k usually extended in a range 10–30 Å^{-1}. β, and β' run over the chemical species of the (multi-component) system, while ρ_β ($\rho_{\beta'}$) are the corresponding partial atomic densities. The irreducible two-body (pair) $\gamma_\beta^{(2)}(k, r)$ signals are oscillating functions in k (leading phase is $2kr$) with an amplitude rapidly decreasing with the interatomic distance r, and can be calculated directly for example with the `gnxas` program (Di Cicco, 2009). Three-body $\gamma_{\beta\beta'}^{(3)}(k, r_1, r_2, \theta)$ signals depend on triangular coordinates (being r_1, r_2 usually the shortest interatomic distances and θ the angle among them). They are also oscillating functions rapidly decaying for increasing distances, with notable exceptions (for example collinear configurations). Eq. (1) truncated to the pair distribution (n= 2) is usually a reasonable approximation for highly disordered systems in the EXAFS regime and $\gamma_\beta^{(2)}(k, r)$ may be approximated by its single scattering expression for large k values.

Accurate and fast calculations of the $\gamma^{(n)}$ signals (through GNXAS) are available so the problem of EXAFS structural refinements consists in finding the best approximation for the g_n distribution functions reproducing the experimental XAS signal $\chi(k)$. However, reliable structural refinements are also related to the correct identification of $\chi(k)$ in raw experimental data usually found in terms of an absorption coefficient $\alpha(E)$, E being the photon energy ($E = EE + \hbar^2k^2/2\,m$ at a selected energy edge EE). The XAS structural signal is experimentally defined as: $\chi(E) = [\alpha(E) - \alpha_{bkg}(E)]/\alpha_0(E)$. The correct modelling of the background $\alpha_{bkg}(E)$ and normalization $\alpha_0(E)$ functions is particularly important especially when dealing with low-intensity $\chi(k)$ oscillations in EXAFS spectra, typical of disordered systems. The atomic absorption can be safely approximated by $J\sigma_0(E)$, where $\sigma_0(E)$ is a decreasing smooth function of the energy as given by a hydrogenic model or by the McMaster compilation (J being the scaling factor accounting for the surface density of the photoabsorbers for XAS in transmission mode). The background shape $\alpha_{bkg}(E)$ depends on the particular experiment and can be usually approximated by piece-wise polynomial functions, but can also contain step-like explicit contributions associated with multielectron excitation channels (see for example Di Cicco et al., 1992, 2000; Filipponi and Di Cicco, 1995a, 1995b). For what concerns the EXAFS structural refinement, GNXAS usually employs a simple peak-fitting technique. In fact, pair and higher-order distribution functions can be modelled as sums of distinct Gaussian or slightly asymmetric peaks, an approximation useful for most solid systems and computationally fast. This approach is implemented in the program `fitheo` which provides the structural refinement in terms of parameters defining the distribution functions (Di Cicco, 2009). More details are given in many previous works (see for example Filipponi and Di Cicco, 1995a) but here I just recall that the approach used in GNXAS refinements (i.e. minimizing the difference of the model $\alpha_{mod}(E)$ and experimental $\alpha(E)$ absorption spectra) is particularly efficient and statistically sound. Using the `fitheo` routine, background and non-structural parameters are optimized together with the local structure searching a solution in the entire parameters' space. In previous works, the use of raw EXAFS $\alpha(E)$ absorption data has been found to be extremely useful to avoid systematic errors in the structural refinement, due to incorrect background modelling, and to assess realistic uncertainty values to the structural parameters as a consequence of the noise level in the measurements. In particular, best-fit values for the structural parameters and error bars (including correlation maps) can be defined using raw data with no Fourier filtering. The accuracy in the structure refinement obtained by single and multiple-edge XAS studies, using multiple-scattering peak-fitting techniques, has been assessed in molecular gas-phase and crystal system by direct comparison with diffraction data (see for example Di Cicco et al., 1992; Filipponi and Di Cicco, 1995a; Filipponi and D'Angelo, 1998 and refs. therein). Typical accuracy in the determination of local interatomic distances can easily reach 0.002 Å while new information on bond-angle distribution and correlated vibrational amplitudes can be obtained by XAS.

For disordered systems, the peak-fitting approach for structural refinement can show severe limitations. For example, it has been shown that for simple liquids XAS refinement must include suitable constraints for medium and long-range structure. Filipponi and Di Cicco (1995b), Filipponi (2001), Di Cicco (2009) These constraints can be introduced for mono-atomic (Filipponi, 1994) and binary liquids (Trapananti and Di Cicco, 2004) in the framework of the peak-fitting technique, and proper subroutines were included in the `fitheo` program (GNXAS) (Di Cicco, 2009) accounting for the correct long-range behavior of the pair distribution functions. It is important to remark that refinements of the local structure of liquids neglecting those constraints can lead to misleading or erroneous results. In a typical close-packing liquid like Pb, for example, the first-neighbor coordination number was found to decrease to about 50% the value known from x-ray and neutron diffraction crystalline, using a simple non-constrained peak-fitting approach (Stern et al., 1991). The reason for such a discrepancy is related to the strong correlation between standard XAS peak-fitting parameters (coordination N and bond variance σ^2) but this example epitomizes the importance of a correct XAS data-analysis and treatment of disorder. As shown in many successive papers, the pair distribution obtained by XAS using modern data-analysis methods like GNXAS was shown to be consistent and in excellent agreement with previous estimates (see the next Section 3 and simple examples like Ge, Filipponi and Di Cicco, 1995b and Ga Di Cicco and Filipponi, 1994). In the case of liquid Pb (see ref. Witkowska et al., 2006), XAS was found to be consistent with previous diffraction data and was also used to discriminate between various models in light of the XAS sensitivity to the short-range structure. As an example of the importance of application of those techniques to liquid systems I also recall the important improvement in our understanding of the short-range structure in molten salts (see Di Cicco et al., 1997 and refs. therein).

Reverse Monte Carlo (RMC) refinements (Di Cicco et al., 2003, 2018; Di Cicco and Trapananti, 2005) were also used to build realistic models of the tridimensional structure of disordered systems, overcoming the limitations of the model-dependent peak-fitting technique. Within this approach, the model structure associated with the positions of $10^2 - 10^4$ atoms in a box is refined until reaching a satisfactory agreement between a set of calculated and experimental observables (for example EXAFS). The `rmcxas` program of the RMC-GNXAS package is fully interfaced with GNXAS (Di Cicco, 2009) and can perform RMC refinements of both molecular and condensed (ordered or disordered) structures. The χ^2 residual function defined at each RMC step is:

$$\chi^2 = \sum_{n=1}^{N_{EDGE}} \sum_{i=1}^{N_{XAS}} \frac{[\chi_n^E(k_i) - \chi_n^C(k_i)]^2}{\sigma_{n,i}^2} + \sum_{\alpha,\beta} \sum_{j=1}^{N_g} \frac{[g_{\alpha\beta}^E(r_j) - g_{\alpha\beta}^C(r_j)]^2}{\sigma_{\alpha\beta,j}^2} \quad (2)$$

Two main terms contribute to the calculation of the residual function. The first is related to the refinement of the EXAFS $\chi_n^E(k)$ signals using calculated contributions $\chi_n^C(k)$. Multiple-edge refinement is especially important for multiatomic systems so n runs over several (*NXAS*) core-edge spectra and i over the energy points. The second term in Eq. (2) corresponds to the partial pair distribution functions $g_{\alpha\beta}^C$ (α, β are the chemical species) calculated from atomic coordinates and compared with model distributions $g_{\alpha\beta}^E$ obtained from x-ray/neutron diffraction or computer simulations. This term may be substituted with the total pair distribution when partials are not available. For molecules, refinement of the pair distributions can be omitted or substituted with the radial distribution measured for example by electron diffraction. In both terms, the weighting is provided by σ^2 noise functions (possibly evaluated by `fitheo` for the EXAFS spectra).

For condensed matter, the model structure is obtained using a selected number of unit cells and periodic boundary conditions are applied to overcome finite size effects. For molecular systems, the structure is an ensemble of many molecular replicas which provides the necessary configurational average. The method has been validated on simple molecular and multi-atomic systems (Di Cicco and Trapananti, 2005; Di Cicco et al., 2018; Iesari et al., 2018) and applied to the determination of the local structure of liquids (Di Cicco et al., 2003, 2006a, 2014a; Di Cicco and Trapananti, 2007; Iesari and Cicco, 2016).

It has been shown that reliable model-independent pair distribution functions can be extracted by RMC refinements (Di Cicco et al., 2003, 2006a, 2014a; Di Cicco and Trapananti, 2007; Iesari and Cicco, 2016) considering both EXAFS and diffraction $g(r)$ data, for short and medium-long range correlations respectively. In Fig. 1 I report the results of the RMC refinement (864 atoms) of the EXAFS spectrum of liquid Sn (Di Cicco et al., 2006a) as an example. The trend of the χ^2 residual function (defined in Eq. (2)) shows that convergence to the expected value can be reached within a reasonable number of RMC moves. A crucial point for faster convergence is the preparation of an initial structure compatible with the pair distribution function g_2^E chosen for the minimization in Eq. (2). In Fig. 1, lower-right panel, we report the bond-angle distribution of liquid Sn as obtained by the atomic positions of the equilibrated configurations. The bond-angle distribution shows clear differences with that of a typical close-packing liquid (Cu), in which a sizable fraction is due to nearly icosahedral configurations. Details of this study and its relevance for understanding the structure of liquid metals can be found in refs. Di Cicco et al. (2003, 2006a, 2014a), Di Cicco and Trapananti (2007), Iesari and Cicco (2016).

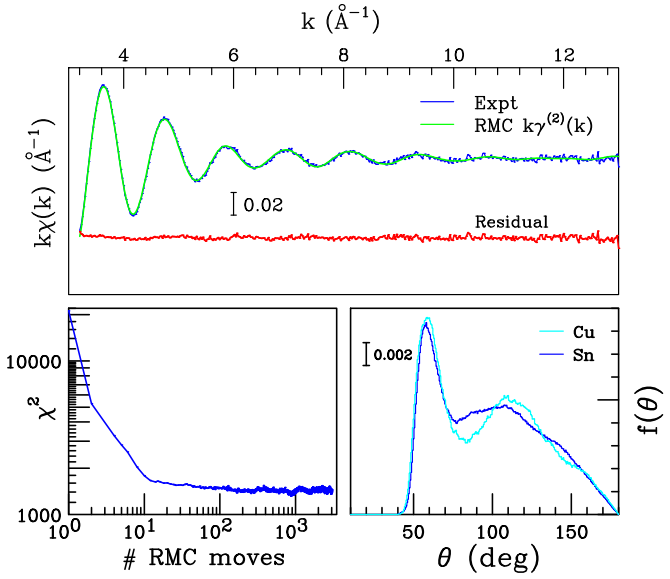

Fig. 1. Upper panel: comparison of the structural XAS signal $k\chi(k)$ measured for liquid Sn (Expt blue curve, T ~ 530 K, P ~ 0.05 GPa) with the result of a Reverse Monte Carlo simulation (RMC green curve, $k\gamma^{(2)}(k)$). The agreement can be appreciated looking at the residual curve (red). Lower-left panel: trend of the χ^2 residual during the RMC simulation procedure. Convergence for this 864-atoms box is reached after $10^2 - 10^3$ RMC moves (each RMC move includes attempts of moving each atom in the box). Lower-right panel: comparison of the normalized bond-angle distribution $f(\theta)$ of liquid Sn, corresponding to the RMC equilibrium configurations, with that of a close-packing liquid (Cu).

3. XAS for glasses and liquids

The application of XAS to condensed systems lacking crystalline order dates back to the early times of this spectroscopy, and contributed also to clarify the short-range nature of the technique. XAS was first used to investigate the structure of amorphous systems (NiS alloys and Ge) in the late 50 s (Sawada et al., 1955; Shiraiwa et al., 1957), and research continued later on (see for example Nelson et al., 1962), until the publication of the seminal paper (Sayers et al., 1971) describing the application of the Fourier Transform technique for investigating non-crystalline structures (applied to amorphous Ge). For a detailed account of early XAS experiments, readers are referred to refs. von Bordwehr and Brouder (1989), Filipponi (2001), while an account of pioneering experiments carried out on liquid and amorphous systems in the first 15 years of synchrotron radiation experiments is contained in Crozier et al. (1988).

In this work, I will briefly show some selected results obtained for simple glasses and liquids that required substantial advances in experimental and data-analysis techniques. Important open scientific problems addressed by those XAS experiments include the presence of icosahedral ordering in close-packed liquids (Di Cicco et al., 2003) and the occurrence of polyamorphism in glasses (Di Cicco et al., 2008; Properzi et al., 2015).

Glasses and amorphous systems have been investigated since the advent of XAS spectroscopy and, during the last decade, several XAS experiments were performed on glasses under high pressure conditions, taking advantage of the advances favoring the performance of reliable and accurate experiments under extreme conditions. Significant efforts were devoted to the study of transformations of the local structure in glasses under pressure, hunting peculiar transitions between low-density (LDA) and high-density (HDA) amorphous structures. Early examples include the fourfold to sixfold coordination change in glassy GeO_2 probed by XAS (Itié et al., 1989), followed by several other studies on similar systems. Recently, evidence of glass polymorphism was obtained by XAS in amorphous Ge (Principi et al., 2004; Di Cicco et al., 2008) under high pressure. As shown in Fig. 2, a well-defined transition is observed increasing pressure as monitored by changes in the first-neighbor distribution parameters. An LDA-HDA (semiconductor to metal) sharp transition has been observed at about 8 GPa by combining XAS, Raman scattering, and XRD techniques, Di Cicco et al. (2008), Coppari et al. (2009, 2012) also confirmed later by ab-initio calculations (Mancini et al., 2015). The transition among two disordered (LDA and HDA) structures can be clearly observed looking at Fig. 2, where an increase of first-neighbor distances R and bond variance σ^2 is observed at the transition point. The nearest neighbor coordination number increases from 4 to ~ 6 from 8 to 10 GPa following the abrupt change of structure. Upon further compression the HDA transform to an ordered GeII phase as can be also seen by the trend observed in the pair distribution function reported in Fig. 2.

XAS has been also applied for understanding the evolution of short-range ordering in compressed archetypal chalcogenide glasses like

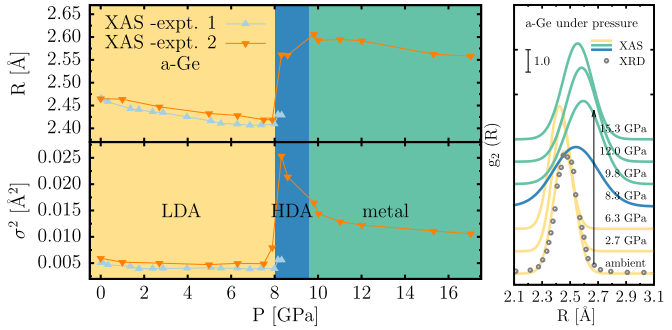

Fig. 2. Left: first-neighbor distance (upper) and bond variance (lower) pressure trend for amorphous Ge under pressure, resulting from 2 XAS experiments using different samples and set-up (Expt 1 Principi et al., 2004, Expt 2 Coppari et al., 2009). The different colors indicate the regions where low-density (LDA) and high-density (HDA) amorphous, as well as solid GeII metal are found for increasing pressures. The nearest-neighbor coordination changes from 4 to 6 in this range. Right: evolution of the first-neighbor pair distribution function for increasing pressure. The pair distribution obtained by XRD experiments Temkin et al. (1973) at ambient pressure is shown for comparison. The curves corresponding to the different LDA, HDA and GeII structures are shown using the same colors of the left panel.

$GeSe_2$ and As_2Se_3 (Properzi et al., 2015, 2016). The effect of compression on the local ordering around both atomic species (Ge, Se in $GeSe_2$) was studied by using a combination of double-edge XAS and XRD experiments (Properzi et al., 2015) and represents an example of gradual LDA to HDA transitions.

In Fig. 3 (left panel) we compare the Ge K-edge XAS structural signals ($\chi(k)$) for crystalline (c-$GeSe_2$) and amorphous (a-$GeSe_2$) materials, as an example of the high-quality and energy extension of the experiments. Se K-edge data are of very similar quality (Properzi et al., 2015) and were used for structural double-edge GNXAS refinements (Di Cicco, 1996; Di Cicco et al., 2000). This analysis provides direct information on the (partial) pair distribution functions (Ge-Se, Se-Se, Ge-Ge, see Fig. 3, center panel). The first neighbor distribution related to the Ge-Se covalent bonding is associated with the dominant Ge-Se (Se-Ge) signals reproducing most of the EXAFS spectral features both for c-$GeSe_2$ and a-$GeSe_2$. For c-$GeSe_2$ the first-neighbor distribution is found

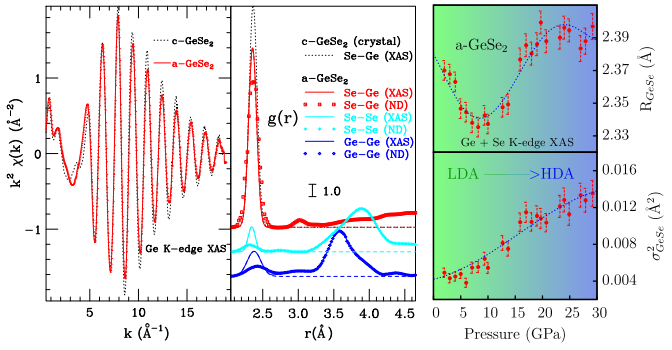

Fig. 3. The Ge K-edge XAS signals of crystalline (c-$GeSe_2$, dots) and amorphous (a-$GeSe_2$) are compared in the left panel. Differences in the low k region and in the XAS amplitude are related to the different short-range ordering of the two systems. The Se-Ge, Ge-Ge, and Se-Se partial pair distribution functions in a-$GeSe_2$ as measured by multiple-edge XAS and neutron-diffraction (ND) are shown and compared with the Ge-Se distribution in c-$GeSe_2$ (center panel). The results of a double-edge XAS refinement of the first-neighbor Ge-Se distance (R_{GeSe}) and bond variance (σ^2_{GeSe}) are shown in the right hand-side panel as a function of pressure for a-$GeSe_2$. The material remains amorphous at all pressures and a transition from a low-density (LDA) to a high-density amorphous (HDA) takes place upon pressurization, as monitored by the change of slope in the bond distance between 10 and 15 GPa. The color gradient is a guide for the eye.

to be in agreement with the known crystal structure (see Ref. Grzechnik et al., 1998 and refs. therein), with given coordination numbers ($N_{GeSe} = 4$, $N_{SeGe} = 2$). Average Ge-Se first-neighbor distance and bond variance were found in substantial agreement with previous EXAFS analysis conducted on Ge-Se glasses (Zhou et al., 1991). Due to the intrinsic short-range nature of the XAS probe, only first-neighbor $g(r)$ peaks (below 2.5 Å in Fig. 3) are accurately measured, but present XAS structural refinement anyway confirms previous ND results (Petri et al., 2000; Salmon and Petri, 2003) about the presence of chemical disorder in $GeSe_2$, indicating that the bond distributions of like-like and like-unlike first-neighbors are well-defined peaks associated with nearly-covalent bonding (Properzi et al., 2015).

The evolution of the local structure of a-$GeSe_2$ with pressure was studied combining dispersive XAS and XRD measurements up to ~ 30 GPa. The sample was found to remain amorphous up to the highest pressures attained, and a reversible red-shift of the Ge K-edge energy, of about 1.5 eV, was observed above 10 GPa up to about 15 GPa (Properzi et al., 2015). This shift is interpreted as the signature of a metallization process associated with the appearance of delocalized electron states mostly around the Ge sites (a similar shift was not observed at the Se K-edge).

The first-neighbor Ge-Se average distance R_{GeSe} probed by XAS is first decreasing and then increasing for pressures above 10 GPa as shown in Fig. 3 (right-hand panel). In the lower portion of Fig. 3, I report also the Ge-Se bond variance σ^2_{GeSe}. The bond variance, associated with structural disorder, is found to increase in the entire pressure range. This is an expected behavior for an amorphous material when further atoms has to be accommodated at short distances by compression, breaking the more ordered and symmetric fourfold coordination (Ge sites). A gradual increase in the first-neighbor coordination number is predicted by MD simulations (Durandurdu and Drabold, 2002), and the mean Ge-Se coordination is estimated around 4.5 at 9.3 GPa by XRD (Mei et al., 2006), reaching ~ 5.5 at about 30 GPa (Durandurdu and Drabold, 2002). The first-neighbor coordination increase upon pressurization is accompanied by a corresponding increase in the average first-shell distance as observed by XAS. The fact that the bond variance (mean square relative displacement) is found still to increase at limiting pressures is seen as an evidence that the conversion to the octahedral configuration (HDA) is not yet completed. This result is in agreement with previous MD simulations (Durandurdu and Drabold, 2002), predicting a full conversion to octahedral coordination only at pressures around 50 GPa. Generally speaking, the compaction mechanism seems to be analogous to what happens in similar systems such as GeO_2 and GeS_2 (Itié et al., 1989; Vaccari et al., 2010).

For liquids, the XAS technique was applied to several molten metals (elemental and alloys), molten salts, molecular liquids, and liquid solutions (see the review Filipponi, 2001 and refs. therein for details). Initial XAS experiments were limited to temperatures reachable with readily available devices (cryostats and furnaces for moderate high temperature around 700 K) but the success of these initial efforts, including production of the first samples of nearly-uniform thickness, leaded soon to the development of a new furnace for x-ray experiments (Filipponi and Di Cicco, 1994; Di Cicco and Filipponi, 1996). Suitable XAS samples of liquid systems were mostly obtained by mixing the investigated substances in form of fine powders (or droplets) with low x-ray absorbing non-reacting materials (typically ultrapure boron nitride, carbon,alumina) in the typical form of compressed pellets. Dispersions of pure (liquid) substances were obtained either using starting ultrapure materials or by in-situ reduction processes at high temperature. For example, extremely good samples for Cu K-edge XAS of liquid copper were obtained by in-situ reduction of copper oxide (mixed with graphite or BN).

A crucial development for the study of order-disorder (and back) phase transitions in condensed matter was the availability of advanced beamlines (Filipponi et al., 2000) including several x-ray data collection modes and suitable sample diagnostics (temperature/pressure). The

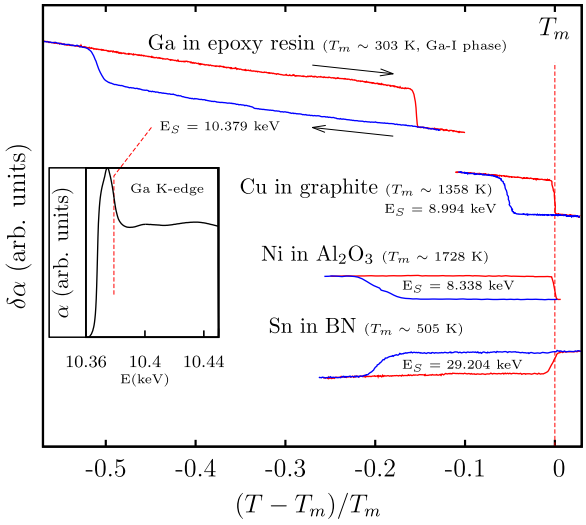

Fig. 4. Single-energy x-ray absorption temperature scans for different metals (see refs. Di Cicco et al., 1999, 2003, 2014a, 2006a), reported on a temperature scale normalized to the melting point T_m of each metal (Ga, Cu, Ni, Sn, see figure). Photon energy for the scans were chosen to maximize the contrast $\delta\alpha$ between liquid and solid phases, in the vicinity of the K-edge of each metal (Ga case is reported in the inset). Depending on the chosen energy point, positive (Sn) or negative (Ga, Cu, Ni) $\delta\alpha$ step-like variations are observed at the melting points. Large undercooling rates are observed in dispersion of (sub)micrometric metal droplets as shown by the hysteresis loops in the figure (heating and cooling are shown as red and blue lines respectively). Undercooling rates depend strongly on the metal, droplet dimensions and of the material used as a container (epoxy resin, graphite, alumina, BN for Ga, Cu, Ni and Sn respectively). The exceptional undercooling of Ga Di Cicco (1998) is due to the peculiar ice-type behavior of this element and the shift of melting point is due to its confinement in epoxy resin.

possibility of collecting high-quality XAS, x-ray diffraction and temperature scans was found to be necessary to pin phase transition points and have full control of the experiments. In fact, the technique of collecting x-ray single-energy temperature scans (Filipponi et al., 1998) was shown to be effective to detect phase transitions and hysteresis loops in ordered and disordered systems.

The possibility of achieving extremely high undercooling rates for elemental liquid systems was soon recognized, in polymorphic low-melting point metals like Ga and Hg. Emulsions of Ga droplets in epoxy resin were found to show exceptional undercooling down to 150 K, and a combination of techniques was used for this purpose (XAS, single-energy temperature scans, XRD, electrical resistivity) (Di Cicco, 1998; Di Cicco et al., 1999). In Fig. 4 I report some x-ray single-energy temperature results obtained for dispersions of metal droplets (grains when crystalline) in different hosting materials. Typically, the photon energy is chosen in the vicinity of the absorption edges, maximizing the contrast among the XAS signals associated with the different phases. In Fig. 4, the temperature scale has been normalized to the (very different) melting points (T_m = 303, 505, 1358, 1728 K, for Ga, Sn, Cu, Ni respectively) in order to compare directly the undercooling rates. As shown in Fig. 4, sharp transitions are observed at the melting points, while re-crystallization takes place usually more gradually at much lower temperatures. Undercooling limits and shape of the crystallization curve depend on various factors including distribution, dimension and shape of the metal particles, purity, and interaction with the hosting material. The remarkable undercooling record obtained for Ga (150 K) was obtained by mixing submicrometric Ga droplets with epoxy resin, and the lowering of melting point to about 254 K is due to the confinement of Ga grains (Di Cicco, 1998) which prevents crystallization to the stable Ga-I (α) phase having a lower density than liquid Ga. Single-energy temperature scans of liquid Cu and Ni shown in Fig. 4 were collected using a high-temperature furnace (Filipponi and Di Cicco, 1994; Di Cicco et al., 2006b, 2014a) developed for combined XAS and XRD measurements. Cu and Ni show quite different undercooling rates in this example, but this is likely to be due mostly to the different materials used as a container (graphite and alumina), which may favor formation of crystal seeds, and to the different droplet size distributions. The hysteresis loop reported in Fig. 4 for Sn powders embedded in boron nitride was obtained at a pressure of 0.05 GPa in the context of a high-pressure XAS experiment (Di Cicco et al., 2006a) discussed below.

As previously mentioned, XAS provided important insights about the local structure in many "simple" liquid systems and demonstrated to stand as a reliable and accurate complementary tool for more standard techniques like x-ray and neutron diffraction. For example, double-edge XAS structural refinement in liquid CuBr was shown to improve significantly our knowledge of local structure provided only by time-consuming isotope-substitution neutron diffraction data. Di Cicco et al. (1997) In simple elemental liquids, the use of RMC structural refinement combining XAS and diffraction data allowed us to provide realistic tridimensional models of the average liquid structure. An example is shown in Fig. 1, in which an EXAFS Sn K-edge spectrum of liquid tin (Di Cicco et al., 2006a) is successfully analysed using RMC. The ensemble of equilibrated atomic configurations of the chosen simulation box reproduces the medium and long-range behavior of the $g(r)$ but new information about the local geometry can be retrieved. The bond-angle distribution shown in Fig. 1 is really different from that of close-packing liquids (Cu, Ni for instance) and a careful analysis shows that the average structure is a mixture of tetrahedral-like and close-packed configurations.

Liquid Sn has been also studied by XAS under high-pressure (Di Cicco et al., 2006a), showing that there is an abrupt change in the undercooling limit above 2 GPa, where nucleation takes place into the Sn-III (metastable) solid phase. At high pressures, local close-packing configurations are found to dominate over the tetrahedral ones favoring crystallization to the Sn-III solid phase stable at higher pressures. This is just an example of XAS studies under high pressures that are now becoming more popular. In fact, excellent XAS spectra can be nowadays obtained for materials under static pressures in the 10 GPa range with large-volume cells and in the MBar range (100 GPa) using diamond anvil cells (see for example Di Cicco and Filipponi, 2015 and refs. therein). Moreover, metastable states including deep undercooled liquids under static pressure can be measured by XAS using well-established techniques (see for example Di Cicco et al., 2006a; Principi et al., 2006) opening scientific explorations of high-pressure metastable states that were previously impossible.

It is worth also to mention that liquids and highly-excited systems can be also probed by XAS under transient conditions with various ultrafast techniques (Bressler and Chergui, 2004), using time-resolved spectroscopies at synchrotron beamlines (see for example refs. Johnson et al., 2005; Cho et al., 2011) or at free-electron laser facilities (see for example refs. Allaria et al., 2012; Obara et al., 2014; Di Cicco et al., 2014b; Principi et al., 2016). Last but not least, the possibility opened by new sources and beamlines of measuring low-noise x-ray Raman (inelastic x-ray scattering, IXS) spectra is also attracting considerable interest for materials containing light elements.

An important example is water, a common liquid for which we can find numerous x-ray, neutron diffraction and simulations results in a worldwide longstanding attempt of solving its elusive structure. Diffraction experiments represent the most direct way to determine the O-O, O-H distances. Despite considerable effort and tremendous technical progresses, the reported g_{OO} maxima in liquid water have varied considerably over the past 70 years between 2.73 Å and 2.89 Å. Values above 2.8 Å were consistently reported before the year 2000, the first neutron diffraction experiment of 1982 gave 2.86 Å (Narten et al., 1982) while 2.82–2.88 Å were found in later studies (see Soper et al., 1997 and refs. therein). In 2000, a values of 2.73 Å and hence a

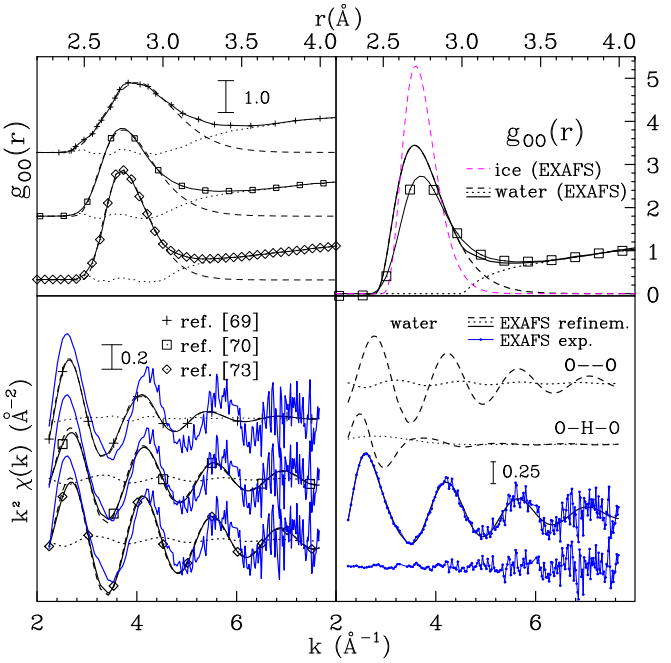

Fig. 5. Upper-left: Comparison of g_{OO} pair distributions obtained by selected x-ray, neutron diffraction and MD simulation studies Soper et al. (1997), Soper (2000), Head-Gordon and Hura (2002), Svishchev and Kusalik (1993). Note the data from Soper (2000) and Head-Gordon and Hura (2002) are very similar (only one is shown). Pair distributions have been decomposed into first-neighbor O-O peaks and a long range O-O tails (dashed lines and dots, respectively). Lower-left: $k^2\chi(k)$ EXAFS structural signal obtained using the $g_{OO}(r)$ s reported in the upper panel (solid and dash curves). For comparison the measured experimental EXAFS (IXS) signal is plotted (blue curve). Upper-right panel: reconstructed g_{OO} using present EXAFS (IXS) O K-edge data for water (solid line) and ice (dashed, magenta). Water g_{OO} has been decomposed in a first-neighbor O-O asymmetric peak (dashed) resulting from the main contribution to the EXAFS structural signal and a long-range tail (dots). The g_{OO} resulting from a previous study Soper (2000) is shown for comparison. Lower-right panel (top to bottom): 1) nearest-neighbor (dashed) and long-range (tail, dots) O–O contributions. 2) intramolecular O-H (dots) and collinear O-H-O (dashed) contributions. 3) EXAFS (IXS) structural signal (blue curve with dots) compared with the best-fit EXAFS refinement (solid). 4) Residual (lower blue curve, dots) showing the level of agreement of present refinement.

distance close to or even smaller than in ice (Ih) has been published (Soper, 2000; Head-Gordon and Hura, 2002). In a more recent work (Brookes and Head-Gordon, 2015), the results of several x-ray diffraction experiments were re-examined showing that a family of g_{OO} curves with maxima in the range 2.75–2.8 Å could provide equally good agreements with high-quality data. Large variations have also been reported using computer simulations that are often found to provide sharper first-neighbor O-O peaks (see for example Svishchev and Kusalik, 1993; Brookes and Head-Gordon, 2015 and refs. therein). In Fig. 5 (upper-left panel) some examples of g_{OO} distributions for liquid water are reported.

Uncertainty in the determination of distance distributions can be traced back to known experimental difficulties (subtraction of background and sample holder contribution, q limits, weak scattering intensities) of the diffraction techniques applied to liquids. Moreover, diffraction does not allow a direct comparison with the local structure of ice (accepted O-O average distance is ~ 2.75 Å in Ih ice) as it can be easily done using XAS. Clearly, the application of XAS is particularly interesting for obtaining a new independent determination of the distribution of distances in ice and water, in view of the XAS chemical selectivity and short-range sensitivity. XAS spectra can be collected at the O K-edge (~ 530 eV photon energy), but soft x-ray absorption techniques are usually strongly surface-sensitive and limited in terms of noise level. Soft x-ray XAS data of liquid water, collected in transmission mode, were shown to contain detectable O-H and O-O contributions (Yang and Kirz, 1987). However, this challenging experiment required ultrathin and homogeneous water droplets and the presence of noise allowed only qualitative comparisons with diffraction data.

Quite recently, we have been able to collect high-quality x-ray Raman XAS measurements (inelastic scattering) of liquid water and polycrystalline ice Ih, using a multicrystal x-ray spectrometer at the undulator beamline 18ID (Advanced Photon Source) in a 6900–7550 eV photon range (energy loss of 439–1089 eV, more details in Bergmann et al., 2007). This technique has the advantage of being a hard x-ray bulk probe also for light elements, but the difficulty of the very small inelastic scattering cross section, overcome in the present experiment by the intense incoming flux and by the efficiency of the spectrometer. The x-ray Raman O K-edge XAS structural signal is compared with the result of multiple-scattering simulations based on diffraction and molecular dynamics pair distributions in Fig. 5 (lower-left panel). XAS calculations were performed within the dipole approximation with the assumption of negligible nondipole x-ray Raman contributions, supported by test calculations (Bergmann et al., 2007). XAS simulations based on those models do not agree with x-ray Raman data so a structural refinement was performed to reconstruct the g_{OO} distribution. The results are shown in Fig. 5 (right-hand panels) and the g_{OO} distribution in water is found to be strongly asymmetric, with a peak position of about 2.70 Å corresponding to a longer average distance of 2.81 Å (as an effect of the skewness of the distribution). The refinement included a small but significant contribution resulting from O-H distances and collinear O-H-O multiple-scattering signal, in agreement with previous indications (Yang and Kirz, 1987). Comparison with previous models for the pair distribution (see Fig. 5) show a small shift to shorter distance and a higher O-O first-peak, but it is important to remark that there is a wide spread in present determinations of the g_{OO} distribution, all in agreement with available diffraction data. (Brookes and Head-Gordon, 2015) This application of the x-ray Raman technique to liquid water shows the high potential of the XAS technique for the reconstruction of the pair distribution and set further restrictions to the range of possible models of liquid water.

Acknowledgments

I kindly acknowledge my research group in Camerino and in particular F. Iesari, L. Properzi and A. Trapananti for their help in this particular work. For most of the results presented in this work I am also deeply indebted to A. Filipponi (Adriano), for his generosity in sharing with me his intuitions, profound understanding of physics, and enthusiasm for experiments and theory. I am also indebted to C. R. Natoli (Rino) who introduced me to the secrets of multiple-scattering calculations and shared with me his “vision” for the connection between theory and experiments. I also kindly acknowledge the PRIN grant (2015) NEWLI provided by the Italian Minister of University and Education.

References

Allaria, E., Battistoni, A., Bencivenga, F., Borghes, R., Callegari, C., Capotondi, F., Castronovo, D., Cinquegrana, P., Cocco, D., Coreno, M., Craievich, P., Cucini, R., D’Amico, F., Danailov, M.B., Demidovich, A., Ninno, G.D., Di Cicco, A., Di Fonzo, S., Di Fraia, M., Di Mitri, S., Diviacco, B., Fawley, W.M., Ferrari, E., Filipponi, A., Froehlich, L., Gessini, A., Giangrisostomi, E., Giannessi, L., Giuressi, D., Grazioli, C., Gunnella, R., Ivanov, R., Mahieu, B., Mahne, N., Masciovecchio, C., Nikolov, I.P., Passos, G., Pedersoli, E., Penco, G., Principi, E., Raimondi, L., Sergo, R., Sigalotti, P., Spezzani, C., Svetina, C., Trova, M., Zangrando, M., 2012. Tunability experiments at the fermi@elettra free-electron laser. New J. Phys. 14, 113009.

Bergmann, U., Di Cicco, A., Wernet, P., Principi, E., Glatzel, P., Nilsson, A., et al., 2007. Nearest-neighbor oxygen distances in liquid water and ice observed by x-ray raman based extended x-ray absorption fine structure. J. Chem. Phys. 127 174504–174504.

von Bordwehr (C.Brouder), R.S., 1989. A history of x-ray absorption fine structure. Ann. Phys. Fr. 14, 377–400.

Bressler, C., Chergui, M., 2004. Ultrafast x-ray absorption spectroscopy. Chem. Rev. 104,

1781–1812.
Brookes, D.H., Head-Gordon, T., 2015. Family of oxygen-oxygen radial distribution functions for water. J. Phys. Chem. Lett. 6, 2938–2943.
Cho, B.I., Engelhorn, K., Correa, A.A., Ogitsu, T., Weber, C.P., Lee, H.J., Feng, J., Ni, P.A., Ping, Y., Nelson, A.J., Prendergast, D., Lee, R.W., Falcone, R.W., Heimann, P.A., 2011. Electronic structure of warm dense copper studied by ultrafast x-ray absorption spectroscopy. 167601. 5. Phys. Rev. Lett. 106. https://doi.org/10.1103/PhysRevLett.106.167601.
Coppari, F., Chervin, J., Congeduti, A., Lazzeri, M., Polian, A., Principi, E., Di Cicco, A., 2009. Pressure-induced phase transitions in amorphous and metastable crystalline germanium by raman scattering, x-ray spectroscopy, and ab initio calculations. Phys. Rev. B 80, 115213.
Coppari, F., Polian, A., Menguy, N., Trapananti, A., Congeduti, A., Newville, M., Prakapenka, V.B., Choi, Y., Principi, E., Di Cicco, A., 2012. Pressureinduced transformations in amorphous si-ge alloy. Phys. Rev. B 85, 045201.
Crozier, E.D., Rehr, J.J., Ingalls, R., 1988. X-Ray absorption: principles. In: Koningsberger, D.C., Prins, R. (Eds.), Applications, Techniques of EXAFS, SEXAFS, and XANES. Wiley, New York, pp. 375–384.
Di Cicco, A., 1996. Multiple-edge exafs refinement: Short-range structure in liquid and crystalline sn. Phys. Rev. B 53, 6174–6185.
Di Cicco, A., 1998. Phase transitions in confined gallium droplets. Phys. Rev. Lett. 81, 2942–2945.
Di Cicco, A. (Ed.), 2009. GNXAS. Extended Suite of Programs for Advanced Xray Absorption Data-analysis: Methodology and Practice. TASK publishing, Gdansk, Poland.
Di Cicco, A., Congeduti, A., Coppari, F., Chervin, J.C., Baudelet, F., Polian, A., 2008. Interplay between morphology and metallization in amorphous-amorphous transitions. Phys. Rev. B 78, 033309. https://doi.org/10.1103/PhysRevB.78.033309.
Di Cicco, A., Filipponi, A., 1994. Local correlations in liquid and supercooled gallium probed by x-ray absorption spectroscopy. Europhys. Lett. 27, 407.
Di Cicco, A., Filipponi, A., 1996. J. Non-Crystall. Solids 205–207, 304–311.
Di Cicco, A., Filipponi, A., 2015. Semiconductors under extreme conditions. In: Schnohr, C.S., Ridgway, M.C. (Eds.), X-Ray Absorption Spectroscopy of Semiconductors. Springer Series in Optical Sciences Springer Berlin Heidelberg, pp. 187–200.
Di Cicco, A., Fusari, S., Stizza, S., 1999. Phase transitions and undercooling in confined gallium. Philos. Mag. B 79, 2113–2120.
DiCicco, A., Gunnella, R., Marassi, R., Minicucci, M., Natali, R., Pratesi, G., Principi, E., Stizza, S., 2006a. Disordered matter under extreme conditions: X-ray diffraction, electron spectroscopy and electroresistance measurements. J. Non-Cryst. Sol. 352, 4155–4165.
Di Cicco, A., Hatada, K., Giangrisostomi, E., Gunnella, R., Bencivenga, F., Principi, E., Masciovecchio, C., Filipponi, A., 2014. Interplay of electron heating and saturable absorption in ultrafast extreme ultraviolet transmission of condensed matter. Phys. Rev. B 90, 220303.
Di Cicco, A., Iesari, F., De Panfilis, S., Celino, M., Giusepponi, S., Filipponi, A., 2014. Local fivefold symmetry in liquid and undercooled ni probed by x-ray absorption spectroscopy and computer simulations. Phys. Rev. B 89, 060102.
Di Cicco, A., Iesari, F., Trapananti, A., DAngelo, P., Filipponi, A., 2018. Structure and atomic correlations in molecular systems probed by xas reverse monte carlo refinement. J. Chem. Phys. 148, 094307. https://doi.org/10.1063/1.5013660.
Di Cicco, A., Minicucci, M., Filipponi, A., 1997. New advances in the study of local structure of molten binary salts. Phys. Rev. Lett. 78, 460–463.
Di Cicco, A., Stizza, S., Filipponi, A., Boscherini, F., Mobilio, S., 1992. Xray absorption investigation of six4 (x= cl, f, ch3). J. Phys. B At. Mol. Opt. Phys. 25, 2309.
Di Cicco, A., Taglienti, M., Minicucci, M., Filipponi, A., 2000. Short-range structure of solid and liquid agbr determined by multiple-edge x-ray absorption spectroscopy. Phys. Rev. B 62, 12001–12013.
Di Cicco, A., Trapananti, A., 2005. Reverse monte carlo refinement of molecular and condensed systems by x-ray absorption spctroscopy. J. Phys.: Condens. Matter 17, S135–S144.
Di Cicco, A., Trapananti, A., 2007. Study of local icosahedral ordering in liquid and undercooled liquid copper. J. Non-Cryst. Sol. 353, 3671–3678. https://doi.org/10.1016/j.jnoncrysol.2007.05.150. (proceedings of the 12th International Conference on Liquid and Amorphous Metals).
Di Cicco, A., Trapananti, A., Faggioni, S., Filipponi, A., 2003. Is there icosahedral ordering in liquid and undercooled metals? PRL 91, 135505–1–135505–4.
Di Cicco, A., Trapananti, A., Principi, E., De Panfilis, S., Filipponi, A., 2006b. Polymorphism and metastable phenomena in liquid tin under pressure. Appl. Phys. Lett. 89, 221912.
Durandurdu, M., Drabold, D.A., 2002. Simulation of pressure-induced polyamorphism in a chalcogenide glass GeS e2. Phys. Rev. B 65, 104208.
Filipponi, A., 1994. The radial distribution function probed by x-ray absorption spectroscopy. J. Phys. Condens. Matter 6, 8415–8427.
Filipponi, A., 2001. Exafs for liquids. J. Phys. Condens. Matter 13, R23.
Filipponi, A., Borowski, M., Bowron, D.T., Ansell, S., Di Cicco, A., De Panfilis, S., Itiè, J.P., 2000. An experimental station for advanced research on condensed matter under extreme conditions at the ESRF - BM29 beamline. Rev. Sci. Instrum. 71, 2422–2432.
Filipponi, A., Borowski, M., Loeffen, P.W., De Panfilis, S., Di Cicco, A., Sperandini, F., Minicucci, M., Giorgetti, M., 1998. Single energy x-ray absorption detection: a combined electronic and structural local probe for phase transitions in condensed matter. J. Phys. Condens. Matter 10, 235–253.
Filipponi, A., D' Angelo, P., 1998. Accurate determination of molecular structures by x-ray absorption spectroscopy. J. Chem. Phys. 109, 5356.
Filipponi, A., Di Cicco, A., 1994. Development of an oven for x-ray absorption measurements under extremely high temperature conditions. Nucl. Instrum. Methods B 93, 302–310.
Filipponi, A., Di Cicco, A., 1995a. Short-range order in crystalline, amorphous, liquid, and supercooled germanium probed by x-ray absorption spectroscopy. Phys. Rev. B 51, 12322–12336.
Filipponi, A., Di Cicco, A., 1995b. X-ray absorption spectroscopy and n-body distribution functions in condensed matter (II): data-analysis and applications. Phys. Rev. B 52, 15135.
Filipponi, A., Di Cicco, A., Natoli, C.R., 1995. X-ray absorption spectroscopy and n-body distribution functions in condensed matter (I): theory. Phys. Rev. B 52, 15122–15134.
Filipponi, A., Di Cicco, A., Tyson, T.A., Natoli, C., 1991. Ab-initio modelling of x-ray absorption spectra. Solid State Commun. 78, 265–269.
Grzechnik, A., Grande, T., St????len, S., 1998. Pressure-induced amorphization of gese2. J. Solid State Chem. 141, 248–254.
Gurman, S.J., Binsted, N., Ross, I., 1986. A rapid, exact curved-wave theory for exafs calculations. J. Phys. C 19, 1845.
Head-Gordon, T., Hura, G., 2002. Chem. Rev. 102, 2651.
Iesari, F., Di Cicco, A., 2016. Local symmetry in liquid metals probed by xray absorption spectroscopy. J. Phys. Conf. Ser. 712, 012038.
Iesari, F., Hatada, K., Trapananti, A., Minicucci, M., Di Cicco, A., 2018. Gnxas: advances in the suite of programs for multiple-scattering analysis of x-ray absorption data, in: S´ebilleau, D., Hatada, K., Ebert, H. (Eds.), Multiple Scattering Theory for Spectroscopies. Springer International Publishing. volume 204 of Springer Proceedings in Physics, pp. xxx–xxx.
Itiè, J.P., Polian, A., Calas, G., Petiau, J., Fontaine, A., Tolentino, H., 1989. Pressure-induced coordination changes in crystalline and vitreous geo2. Phys. Rev. Lett. 63, 398–401. https://doi.org/10.1103/PhysRevLett.63.398.
Itiè, J.P., Polian, A., Martinez-Garcia, D., Briois, V., Di Cicco, A., Filipponi, A., San Miguel, A., 1997. X-ray absorption spectroscopy under extreme conditions. J. Phys IV 7, C2–31.
Johnson, S.L., Heimann, P.A., MacPhee, A.G., Lindenberg, A.M., Monteiro, O.R., Chang, Z., Lee, R.W., Falcone, R.W., 2005. Bonding in liquid carbon studied by time-resolved x-ray absorption spectroscopy. Phys. Rev. Lett. 94, 057407.
Mancini, G., Celino, M., Iesari, F., Cicco, A.D., 2015. Glass polymorphism in amorphous germanium probed by first-principles computer simulations. J. Phys. Condens. Matter 28, 015401.
Mathon, O., Occelli, F., Lescoute, E., Sollier, A., Loubeyre, P., Helsby, W., Headspith, J., Torchio, R., Kantor, I., Pascarelli, S., 2016. High pressure dynamic xas studies using an energy-dispersive spectrometer. High Press. Res. 36, 404–418.
Mei, Q., Benmore, C., Hart, R., Bychkov, E., Salmon, P., Martin, C., Michel, F., Antao, S., Chupas, P., Lee, P., Shastri, S., Parise, J., Leinenweber, K., Amin, S., Yarger, J., 2006. Topological changes in glassy GeSe2 at pressures up to 9.3GPa determined by high-energy x-ray and neutron diffraction measurements. Phys. Rev. B 74, 014203. https://doi.org/10.1103/PhysRevB.74.014203.
Narten, A.H., Thiessen, W.E., Blum, L., 1982. Science 217, 1034.
Nelson, W.F., Siegel, I., Wagner, R.W., 1962. K x-ray absorption spectra of ge in crystalline and amorphous geo2. Phys. Rev. 127, 2025–2027.
Newville, M., Ravel, B., Haskel, D., Rehr, J., Stern, E., Yacoby, Y., 1995. Analysis of multiple-scattering {XAFS} data using theoretical standards. Phys. B Condens. Matter 208-209, 154–156 (proceedings of the 8th International Conference on X-ray Absorption Fine Structure).
Obara, Y., Katayama, T., Ogi, Y., Suzuki, T., Kurahashi, N., Karashima, S., Chiba, Y., Isokawa, Y., Togashi, T., Inubushi, Y., Yabashi, M., Suzuki, T., Misawa, K., 2014. Femtosecond time-resolved x-ray absorption spectroscopy of liquid using a hard x-ray free electron laser in a dual-beam dispersive detection method. Opt. Express 22, 1105–1113.
Petri, I., Salmon, P.S., Fischer, H.E., 2000. Defects in a disordered world: The structure of glassy gese2. Phys. Rev. Lett. 84, 2413–2416.
Principi, E., Di Cicco, A., Decremps, F., Polian, A., De Panfilis, S., Filipponi, A., 2004. Polyamorphic transition of germanium under pressure. Phys. Rev. B 69, 201201.
Principi, E., Giangrisostomi, E., Cucini, R., Bencivenga, F., Battistoni, A., Gessini, A., Mincigrucci, R., Saito, M., Di Fonzo, S., D'Amico, F., Di Cicco, A., Gunnella, R., Filipponi, A., Giglia, A., Nannarone, S., Masciovecchio, C., 2016. Free electron laser-driven ultrafast rearrangement of the electronic structure in ti. Struct. Dyn. 3, 023604.
Principi, E., Minicucci, M., Di Cicco, A., Trapananti, A., De Panfilis, S., Poloni, R., 2006. Metastable phase diagram of bi probed by single-energy x-ray absorption detection and angular dispersive x-ray diffraction. Phys. Rev. B 74, 064101. https://doi.org/10.1103/PhysRevB.74.064101.
Properzi, L., Di Cicco, A., Nataf, L., Baudelet, F., Irifune, T., 2015. Short-range order of compressed amorphous gese2. Sci. Rep. 5, 10188.
Properzi, L., Santoro, M., Minicucci, M., Iesari, F., Ciambezi, M., Nataf, L., Le Godec, Y., Irifune, T., Baudelet, F., Di Cicco, A., 2016. Structural evolution mechanisms of amorphous and liquid as2se3 at high pressures. Phys. Rev. B 93, 214205.
Rehr, J.J., Mustre de Leon, J., Zabinsky, S.I., Albers, R.C., 1991. Theoretical x-ray absorption fine structure standards. J. Am. Chem. Soc. 113, 5135–5140.
Salmon, P.S., Petri, I., 2003. Structure of glassy and liquid gese 2. J. Phys. Condens. Matter 15, S1509.
Sawada, M., Tsutsumi, K., Shiraiwa, T., Obashi, M., 1955. On the fine structures of x-ray absorption spectra of amorphous substances. J. Phys. Soc. Japan 10, 464–468.
Sayers, D.E., Stern, E.A., Lytle, F.W., 1971. New technique for investigating noncrystalline structure: Fourier analysis of the exafs. Phys. Rev. Lett. 27, 1204–1207.
Shiraiwa, T., Ishimura, T., Sawada, M., 1957. Fine structures of x-ray absorption spectra of crystalline and amorphous Ge. J. Phys. Soc. Japan 12, 788–792.
Soper, A., 2000. Chem. Phys. 258, 121.
Soper, A.K., Bruni, F., Ricci, M.A., 1997. J. Chem. Phys. 106, 247.
Stern, E.A., L¯ıvin¸ˇs, P., Zhang, Z., 1991. Phys. Rev. B 43, 8850.

Svishchev, I.M., Kusalik, P.G., 1993. Structure in liquid water: A study of spatial distribution functions. J. Chem. Phys. 99, 3049–3058.
Temkin, R.J., Paul, W., Connell, G.A.N., 1973. Amorphous germanium ii. structural properties. Adv. Phys 22, 581–641. https://doi.org/10.1080/00018737300101349.
Trapananti, A., Di Cicco, A., 2004. Probing the local structure of liquid binary mixtures by x-ray absorption spectroscopy. Phys. Rev. B 70, 014101.
Vaccari, M., Garbarino, G., Aquilanti, G., Coulet, M.V., Trapananti, A., Pascarelli, S., Hanfland, M., Stavrou, E., Raptis, C., 2010. Structural changes in amorphous GeS 2 at high pressure. Phys. Rev. B 81, 014205.
Witkowska, A., Rybicki, J., Panfilis, S.D., Di Cicco, A., 2006. The structure of liquid lead: {EXAFS} and {MD} studies. J. Non-Crystall. Solids 352, 4351–4355 (proceedings of the 3rd International Conference on Physics of Disordered Systems (PDS 05)).
Yang, B.X., Kirz, J., 1987. Extended x-ray-absorption fine structure of liquid water. Phys. Rev. B 36, 1361–1364.
Zhou, W., Paesler, M., Sayers, D.E., 1991. Structure of germanium-selenium glasses: An x-ray-absorption fine-structure study. Phys. Rev. B 43, 2315–2321.